

# Lone-Pair Stabilization in Transparent Amorphous Tin Oxides: A Potential Route to p-Type Conduction Pathways

Matthew J. Wahila,<sup>†</sup> Keith T. Butler,<sup>\*,‡</sup> Zachary W. Lebens-Higgins,<sup>†</sup> Christopher H. Hendon,<sup>‡,§</sup> Abhishek S. Nandur,<sup>§</sup> Robert E. Trehearne,<sup>||</sup> Nicholas F. Quackenbush,<sup>†</sup> Shawn Sallis,<sup>§</sup> Katie Mason,<sup>†</sup> Hanjong Paik,<sup>‡,¶</sup> Darrell G. Schlom,<sup>‡,¶</sup> Joseph C. Woicik,<sup>¶</sup> Jinghua Guo,<sup>†</sup> Dario A. Arena,<sup>¶,◆</sup> Bruce E. White Jr.,<sup>§</sup> Graeme W. Watson,<sup>○</sup> Aron Walsh,<sup>‡</sup> and Louis F. J. Piper<sup>\*,†</sup>

<sup>†</sup>Department of Physics, Applied Physics and Astronomy, Binghamton University, Binghamton, New York 13902, United States

<sup>‡</sup>Department of Chemistry, University of Bath, Claverton Down, Bath BA2 7AY, United Kingdom

<sup>§</sup>Materials Science and Engineering, Binghamton University, Binghamton, New York 13902, United States

<sup>||</sup>Stephenson Institute for Renewable Energy, University of Liverpool, Liverpool, L69 7ZF, United Kingdom

<sup>‡</sup>Department of Materials Science and Engineering, Cornell University, Ithaca, New York 14853-1501, United States

<sup>#</sup>Kavli Institute at Cornell for Nanoscale Science, Ithaca, New York 14853, United States

<sup>¶</sup>Materials Science and Engineering Laboratory, National Institute of Standards and Technology, Gaithersburg, Maryland 20899, United States

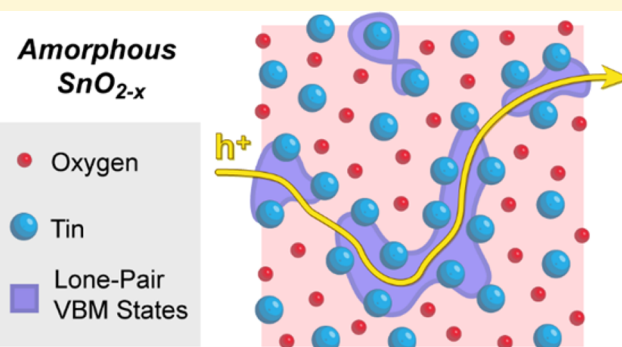
<sup>†</sup>Advanced Light Source, Lawrence Berkeley National Laboratory, Berkeley, California 94720, United States

<sup>▽</sup>National Synchrotron Light Source-II, Basic Energy Sciences Directorate, Brookhaven National Laboratory, Upton, New York 11973, United States

<sup>○</sup>School of Chemistry and CRANN, Trinity College Dublin, Dublin 2, Ireland

## Supporting Information

**ABSTRACT:** The electronic and atomic structures of amorphous transparent tin oxides have been investigated by a combination of X-ray spectroscopy and atomistic calculations. Crystalline SnO is a promising p-type transparent oxide semiconductor due to a complex lone-pair hybridization that affords both optical transparency despite a small electronic band gap and spherical s-orbital character at the valence band edge. We find that both of these desirable properties (transparency and s-orbital valence band character) are retained upon amorphization despite the disruption of the layered lone-pair states by structural disorder. We explain the anomalously large band gap widening necessary to maintain transparency in terms of lone-pair stabilization via atomic clustering. Our understanding of this mechanism suggests that continuous hole conduction pathways along extended lone pair clusters should be possible under certain stoichiometries. Moreover, these findings should be applicable to other lone-pair active semiconductors.



## INTRODUCTION

Hole doping in transparent oxide semiconductors is a long-standing problem due to the deep and localized oxygen 2p states that typically form the valence band edge.<sup>1,2</sup> The directional nature of these p-orbitals makes forming continuous conduction pathways at the valence band edge far more challenging than at the s-orbital derived conduction band edge common in n-type oxides such as IGZO.<sup>3</sup> This problem is particularly pronounced in amorphous materials where lattice networks are distorted and broken. In addition, these O 2p states typically lie too far below the Fermi level in transparent,

wide band gap oxides to allow for straightforward p-type doping.<sup>4–6</sup>

Previous attempts to overcome these issues have involved modulating the valence band edge through hybridization of the O 2p with metal orbitals, such as in the case of CuAlO<sub>2</sub> and its O 2p–Cu 3d hybridization.<sup>7–9</sup> However, the highly directional nature of the commonly utilized orbitals means that structural disorder disturbs this crucial hybridization, severely disrupting

Received: April 20, 2016

Revised: June 8, 2016

Published: June 8, 2016



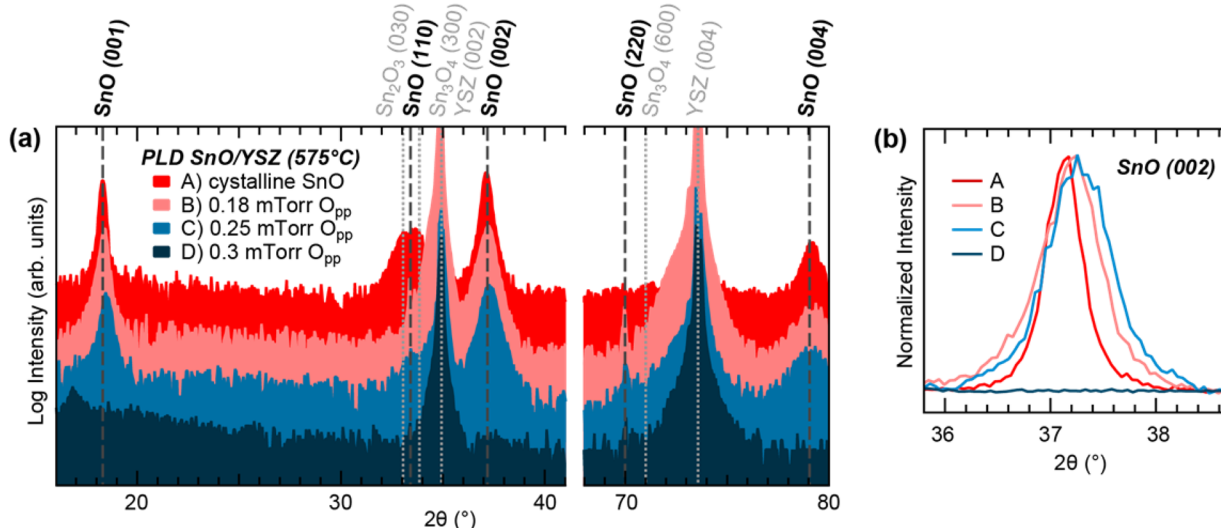


**Figure 1.** (a) X-ray diffraction spectra (regions without peaks have been omitted) of a series of SnO/YSZ thin films grown by pulsed laser deposition. (b) Zoomed in SnO (002) peak showing broadening with increasing oxygen partial pressure.

hole conduction pathways. As such, although possible p-type transparent amorphous oxide semiconductor (TAOS) candidates have been reported, e.g., a-ZnO·Rh<sub>2</sub>O<sub>3</sub><sup>10</sup> and a-ZnCo<sub>2</sub>O<sub>4</sub>,<sup>11–13</sup> no bona fide p-type TAOS materials have been sufficiently demonstrated or commercialized to date.

In this study, we investigate the effects of structural disorder on thin films possessing a stannous oxide (SnO) stoichiometry. SnO and other lone-pair active, post-transition metal oxides can have a raised and delocalized valence band edge due to a complex hybridization between the O 2p and metal s- and p-orbitals.<sup>14–20</sup> Moreover, in SnO this hybridization results in a small (~0.7 eV), indirect, electronic band gap which enables bipolar doping without curtailing optical transparency.<sup>21–23</sup> However, these orbital interactions have only been thoroughly examined within the context of layered crystal structures incorporating a lone-pair distortion. The effects of structural disorder on the orbital hybridizations within these lone-pair active materials have yet to be thoroughly studied and understood.

We find that in contrast to common n-type TAOS materials,<sup>24–27</sup> amorphization of SnO results in an increase in electron stability at the valence band edge with no apparent band gap shrinkage due to deep subgap states. This preserves optical transparency, despite the loss of the indirect/direct band gap distinction present in the crystalline phase. Additionally, we uncover a propensity at this metal rich stoichiometry for tin atoms to form stabilizing clusters which amalgamate the tin lone-pair electron states, similar to the layering and lone-pair distortions in the crystalline phase. This leads to a valence band edge with substantial metal s-orbital character in the amorphous phase. We suggest that this lone-pair clustering has the potential to facilitate the formation of hole conduction pathways in amorphous oxides if stoichiometry and atomic coordination can be properly controlled. This work provides new insight into the interplay between atomistic and electronic structure necessary for developing future p-type TAOS materials.

## ■ RESULTS AND DISCUSSION

Tin monoxide thin films were grown at high temperatures on yttria-stabilized zirconia (YSZ) (001) substrates using pulsed

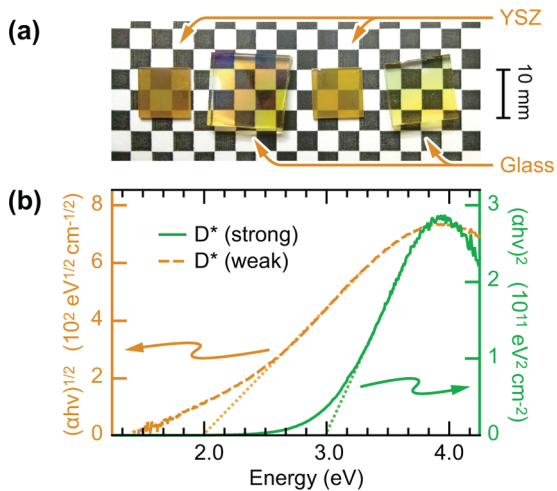
laser deposition (PLD) under an oxygen partial pressure. Room temperature growths on soda-lime glass were also carried out, since low temperature processes on inexpensive substrates would be preferable for the creation of mass produced electronics. The thicknesses of the films were on the order of 100 nm, as determined by cross-sectional scanning electron microscopy.

Figure 1a shows X-ray diffraction (XRD) measurements used to determine film crystallinity. Most films grown at 575 °C on YSZ display peaks attributable to crystalline SnO; however, the degree of crystallinity is highly dependent on the oxygen partial pressure during deposition.<sup>28</sup> The tuning of structural disorder from highly crystalline to fully amorphous is shown by the normalized SnO (002) peaks in Figure 1b. Increasing broadening of the SnO diffraction peaks from samples A to C is observed, indicating a decrease in crystallite size/crystalline quality with increasing oxygen partial pressure. No SnO<sub>x</sub> peaks are observable in the XRD spectra of the sample grown at the highest oxygen partial pressure (sample D) at any sample orientation, indicating full amorphization. Films grown at room temperature on glass were found to be amorphous by XRD and appear nearly identical to the high temperature amorphous films optically and electronically (see Supporting Information for more details).

The electronic properties of the films were also found to trend with oxygen partial pressure. Partially crystalline SnO films were found to be p-type from Hall measurements, while the fully amorphous films could not be accurately measured by the system. The previously reported carrier concentration ( $N_h \sim 1 \times 10^{17} \text{ cm}^{-3}$ ) and hole mobility ( $\mu_h = 7 \text{ cm}^2 \text{ V}^{-1} \text{ s}^{-1}$ ) of Sample A<sup>21</sup> result in a conductivity among the highest reported in the literature for crystalline SnO. Sample B was found to have a higher hole concentration than Sample A ( $N_h = 1.3 \times 10^{18} \text{ cm}^{-3}$ ) but lower hole mobility ( $\mu_h = 1.6 \text{ cm}^2 \text{ V}^{-1} \text{ s}^{-1}$ ). Sample C was found to have an even higher hole concentration ( $N_h = 1.7 \times 10^{18} \text{ cm}^{-3}$ ) and lower mobility ( $\mu_h = 1.2 \text{ cm}^2 \text{ V}^{-1} \text{ s}^{-1}$ ). This is consistent with the formation of additional structural defects due to worsening crystal quality. Consistent Hall measurement results could not be obtained on any of the fully amorphous films, suggesting they are more resistive than the partially crystalline films. However, the Hall effect is known

to be far less straightforward in amorphous materials, especially if polaron hopping plays a large role in the charge transport.<sup>29</sup>

No significant optical changes were observed with the changes in the growth parameters. Amorphous films grown at room temperature still appear optically transparent with a slight yellow hue similar to crystalline SnO,<sup>21</sup> as shown in Figure 2a.



**Figure 2.** (a) Photo of various amorphous SnO thin films on glass and single-polished YSZ. (b) Direct and indirect Tauc plots for an amorphous SnO film on glass ( $D^*$ ).

Film thickness variations are responsible for the gradated appearance of some of the films. An optical band gap of 3 eV was determined from Tauc analysis, with additional weak absorption observed down to approximately 2 eV, as shown in Figure 2b. While the optical gap compares well to the direct band gap of crystalline SnO (~2.7 eV), the weak absorption starting at ~2 eV represents a substantial increase from the electronic gap of crystalline SnO (0.7 eV).<sup>21–23</sup> Although crystalline mixed  $\text{Sn}^{2+}/\text{Sn}^{4+}$  oxides have been found to have band gaps larger than SnO but smaller than  $\text{SnO}_2$ ,<sup>30</sup> no evidence of these crystalline intermediate phases was observed in the XRD spectra of the structurally disordered films.

To confirm that the films possessed the desired SnO stoichiometry and  $\text{Sn}^{2+}$  charge state, X-ray photoelectron spectroscopy (XPS) was performed. From XPS core-level analysis, the high temperature films (A–D) were found to have tin to oxygen ratios of 1:0.85 (A), 1:0.94 (B), 1:0.95 (C), and 1:1.03 (D). An example room temperature amorphous film ( $D^*$ ) was found to have a ratio of 1:0.90. In comparison, reference  $\text{SnO}_2$  films were found to have tin to oxygen ratios of 1:1.62 and 1:2.03 for amorphous and crystalline, respectively. With the exception of sample A and the amorphous  $\text{SnO}_2$  reference, all samples display the expected ratios within the limits of our detection. We note that the seemingly oxygen deficient compositions of these outliers are likely an artifact from our consideration of surface contamination (see Supporting Information for more details). For further analysis we employed synchrotron-based hard X-ray photoelectron spectroscopy (HAXPES), which provides a much deeper

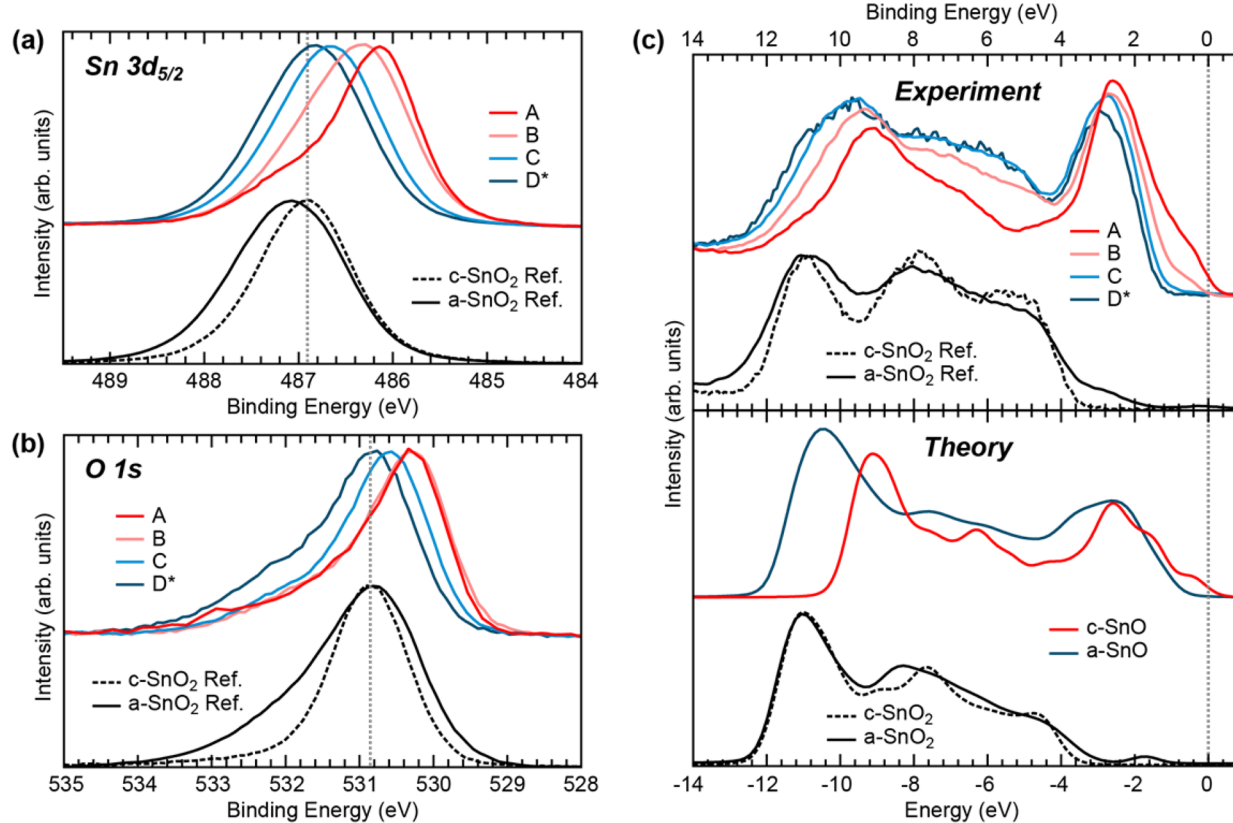


**Figure 3.** (a) HAXPES Sn 3d<sub>5/2</sub> and (b) O 1s core levels of SnO films of varying crystallinity. Vertical dotted lines corresponding to c-SnO<sub>2</sub> peak positions are included to guide the eye. (c) Experimental HAXPES and broadened, orbital cross-section weighted DFT total DOS valence band spectra for SnO films of varying crystallinity. SnO<sub>2</sub> spectra are included for reference. HAXPES spectra for sample A have been reported previously.<sup>21</sup>

probing depth than XPS, thereby reducing the contribution of surface species/contamination to the experimental spectra.

**Figure 3a** shows the spin-orbit split Sn 3d<sub>5/2</sub> core-level of the films measured using HAXPES, including SnO<sub>2</sub> thin film spectra for reference. Unlike the SnO<sub>2</sub> references that both display a single symmetric peak at ~487 eV, the SnO films exhibit large peak shifts with amorphization. While the crystalline SnO displays the Sn 3d<sub>5/2</sub> peak at 486.2 eV, expected for a Sn<sup>2+</sup> charge state,<sup>21,31</sup> the peak shifts toward that of SnO<sub>2</sub> (Sn<sup>4+</sup>) with increasing disorder. Commensurate shifting of the O 1s peak toward that of SnO<sub>2</sub> is also observed, as shown in **Figure 3b**. However, as the SnO films possess the correct ~1:1 stoichiometry and no Sn 3d<sub>5/2</sub> spectral weight associated with under-coordinated Sn<sup>0</sup>, the peak shifts cannot be explained by simple overoxidation or phase separation resulting in Sn<sup>4+</sup>.

The binding energy of a core-level depends on not only the number of valence electrons or charge state but also on the Madelung potential of the photoemitting atom and the electron chemical potential of the compound. Structural disorder will typically produce a wider spread of Madelung potentials, which results in a broadening of the core-level peaks.<sup>24</sup> This peak broadening is clearly evident in the HAXPES spectra of both amorphous SnO and SnO<sub>2</sub>. The large energy shifts of the SnO core-levels are far more likely to result from changes in chemical potential. While the slight shift in peak positions between crystalline and amorphous SnO<sub>2</sub> could reflect a small difference in chemical potential, the more substantial ( $\sim 1$  eV) shifts in the SnO must represent considerable changes to the chemical environment.

Turning to the valence band HAXPES shown in Figure 3c, large transfers of spectral weight are observed in the SnO films with amorphization indicating substantial changes in the interatomic interactions and orbital hybridizations. Also shown in Figure 3c, this evolution of the VBM is reproduced by the DFT calculated total density of states (DOS) after orbital cross-section weighting and broadening to match the instrumental resolution of the HAXPES (see Supporting Information).<sup>21,32</sup> Notably, the shoulder-like feature at the valence band maxima (VBM) of SnO is found to diminish and eventually disappear with increasing structural disorder. This increases the band gap of amorphous SnO by  $\sim$ 1 eV, which allows the amorphous SnO films to maintain the transparency of their crystalline counterparts despite the loss of the indirect/direct band gap distinction (see Supporting Information). Moreover, as depicted in Figure 4a, p-type doping should still be allowed in amorphous SnO despite the 1 eV lowering of the VBM, as it would possess an ionization potential similar to that of p-type CuAlO<sub>2</sub>.<sup>9</sup>

Significant changes to the SnO VBM are somewhat expected as these states are understood to result from an O 2p<sub>z</sub> assisted Sn 5s–Sn 5p lone-pair distortion of the layered litharge crystal structure, depicted in Figure 4b.<sup>14,15</sup> These lone-pair interactions are already known to be highly sensitive to changes in the interlayer distance in layered crystalline tin oxides.<sup>30</sup> The loss of the well-defined crystal layers and structural lone-pair distortions upon amorphization are therefore expected to greatly modify the lone-pair hybridizations. However, it is important to note that comparison between XPS and HAXPES confirms that the topmost valence band retains its tin orbital character upon amorphization, indicating lone-pair hybridization must still play a fundamental role in forming these VBM states (see Supporting Information).

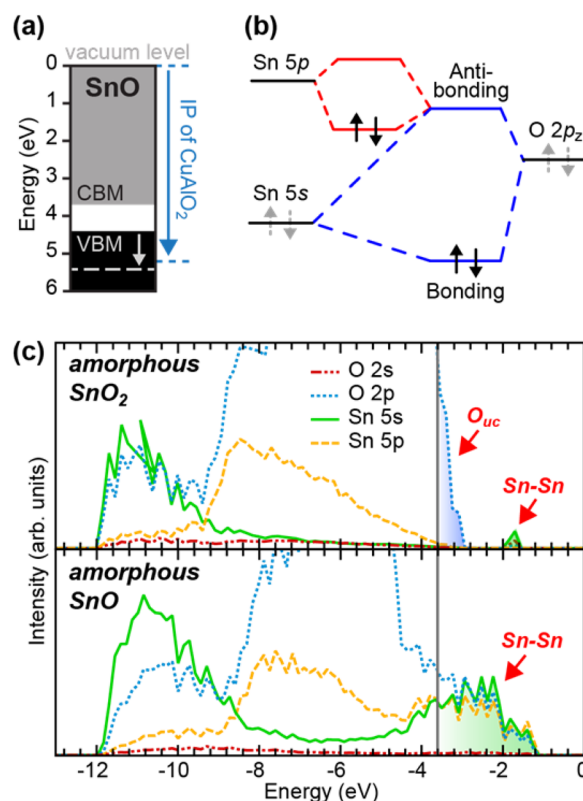


**Figure 4.** (a) Diagram of predicted ionization potential change with amorphization. (b) Simplistic diagram of the orbital interactions leading to lone-pair electrons in crystalline SnO. (c) Unweighted DFT partial DOS of amorphous SnO<sub>2</sub> and SnO.

While states near the VBM are typically attributed to under-coordinated oxygen in other amorphous post-transition metal oxides,<sup>24-26</sup> the metal-rich stoichiometry of SnO means under-coordinated oxygen is unlikely to exist in large quantities. In addition, these oxygen states would typically be ascribed to localized defects caused by the spread in Madelung potentials,<sup>24,26</sup> a phenomena which is insufficient to describe the large VBM feature observed in the amorphous SnO.

Although the role of under-coordinated oxygen in creating subgap states is well documented in  $\text{Sn}^{4+}$  oxide systems (e.g.,  $\text{Zn}-\text{Sn}-\text{O}$ ,  $\text{In}-\text{Sn}-\text{O}$ , etc.), recent calculations have pointed toward  $\text{Sn}-\text{Sn}$  defects as the source of an additional deep subgap state existing  $\sim 1$  eV from the VBM.<sup>33</sup> Shown in Figure 4c, our unweighted calculated partial DOS are in excellent agreement with previous results for amorphous tin oxides, displaying only O 2p related states at the immediate VBM due to under-coordinated oxygen and a Sn 5s character subgap state  $\sim 1$  eV above the VBM due to under-coordinated tin.<sup>33,34</sup>

For amorphous SnO, our calculations suggest O 2p character does not constitute the entirety of the VBM, in agreement with our experimental results. Instead, a mix of both O 2p and Sn 5s–Sn 5p character makes up the topmost valence band states despite the loss of the layered structure. This is consistent with a recent theoretical study on crystalline, single-layer SnO, which suggests the absence of interlayer lone-pair interactions can result in more on-site Sn 5s–Sn 5p hybridization and a consequent widening of the band gap.<sup>35</sup>

The calculated pair distribution functions shown in Figure 5a lend further support to the previous conclusions. For the amorphous  $\text{SnO}_2$ , the calculated coordination number for O—

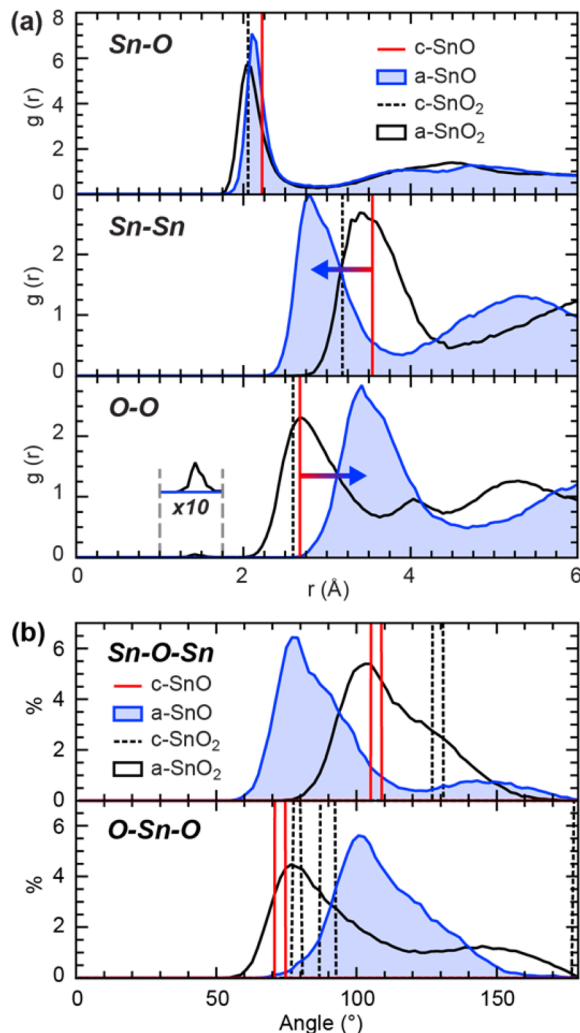


**Figure 5.** (a) Calculated pair distribution functions and (b) calculated bond angle distributions for crystalline and amorphous SnO and SnO<sub>2</sub>.

Sn is 2.98, suggesting a small amount of oxygen undercoordination. Some counterbalancing O–O overcoordination is also observed due to the exact SnO<sub>2</sub> stoichiometry, shown by the small feature at  $\sim 1.4$  Å in the O–O pair distribution function. This is consistent with the observation of undercoordinated oxygen related subgap states in amorphous SnO<sub>2</sub> resulting from a broader spread in Madelung potentials.

For the SnO, far greater changes are observed with amorphization. While the Sn–O distance remains fairly stable with amorphization, barring a slight shift ( $\sim 0.1$  Å) toward that of SnO<sub>2</sub>, the predominant Sn–Sn distance decreases by  $\sim 1$  Å while the O–O increases by  $\sim 1$  Å. This is indicative of a clustering of the tin atoms and spreading out of the oxygen atoms, which would result in a substantial number of Sn–Sn interactions and little to no under-coordinated oxygen.

The calculated bond angle distributions, shown in Figure 5b, also indicate a clustering of tin atoms. For amorphous SnO, the Sn–O–Sn bond angle distribution shows two predominant bond angles (i.e.,  $\sim 70^\circ$  and  $\sim 140^\circ$ ), suggesting an asymmetric distribution of the tin surrounding oxygen atoms. In contrast, only one main O–Sn–O bond angle ( $\sim 100^\circ$ ) is observed, suggesting a more uniform distribution of oxygen around individual tin atoms. Interestingly, the opposite behavior is observed in amorphous SnO<sub>2</sub>, with the Sn–O–Sn and O–Sn–

O showing one ( $\sim 100^\circ$ ) and two ( $\sim 70^\circ$  and  $\sim 140^\circ$ ) main bond angles, respectively. This suggests more oxygen clustering is occurring in the amorphous SnO<sub>2</sub>.

Isosurfaces of the VBM states, shown in Figure 6, strongly support the idea of tin clusters in amorphous SnO. While the oxygen related VBM states in SnO<sub>2</sub> exist localized around oxygen sites, the tin lone-pair related states in amorphous SnO clearly exhibit a propensity to form extended clusters. The states that form these clusters are homologous to those of the Sn–Sn defects in amorphous SnO<sub>2</sub>. However, the metal rich stoichiometry of SnO allows for a much greater number of such states, forming extensive regions of spatial overlap, which lead to significant delocalization of the VBM. As a result, a sufficient density of these clusters could potentially facilitate the creation of continuous hole conduction pathways. Similar electron conduction pathways have been identified in amorphous indium oxide.<sup>36</sup> While this conduction would of course be limited by the charge transfer/hopping between conductive domains, similar to amorphous IGZO or conjugated polymers,<sup>37–39</sup> this issue might be addressed by altering domain extent and interconnectivity through careful control of composition, disorder, and other factors.

## CONCLUSIONS

Structural disorder in SnO is found to facilitate stronger interactions between the Sn 5s and Sn 5p orbitals than might be expected, resulting in a widening of the band gap. These orbital interactions also enable the valence band maximum to maintain substantial metal s-orbital character despite the loss of the lone-pair distorted litharge structure of crystalline SnO. We predict that the resulting valence band maximum of amorphous SnO will have less spatial localization than the O 2p derived valence band maximum of SnO<sub>2</sub> and similar n-type oxides. We propose that this lone-pair stabilization via metal atom clustering may provide a new means to enable continuous hole conduction pathways in amorphous lone-pair active oxides, provided stoichiometry and atomic coordination are properly controlled.

## METHODS

**Sample Growth.** All SnO thin films were grown via pulsed laser deposition (PLD) using a sintered SnO target at the Analytical and Diagnostics Laboratory (ADL) at Binghamton University. Fully amorphous SnO films were grown at room temperature on both molybdenum-coated and uncoated soda-lime glass substrate. Crystalline and partially crystalline SnO thin films were grown epitaxially on a single crystal, (001)-oriented yttria-stabilized zirconia (YSZ) substrate at 575 °C with a fluence of 2 J/cm<sup>2</sup>, as reported previously.<sup>21</sup> Films were grown under a base pressure of  $3 \times 10^{-6}$  Torr with oxygen partial pressures from 1.8 to  $3.0 \times 10^{-4}$  Torr.

The epitaxial SnO<sub>2</sub> reference thin film was grown by codepositing tin and distilled ozone on an atomically smooth single crystal, rutile (110)-oriented TiO<sub>2</sub> substrate via reactive molecular beam epitaxy. The growth was performed at 450 °C under a distilled ozone background pressure of  $1.0 \times 10^{-6}$  Torr. The amorphous SnO<sub>2</sub> reference thin film was grown at room temperature on a glass substrate via RF magnetron sputtering with a SnO<sub>2</sub> target and 5 mTorr Ar partial pressure.

**X-ray Diffraction.** X-ray diffraction (XRD) was performed using a PANalytical X'Pert PRO XRD system. The c-SnO and c-SnO<sub>2</sub> references displayed the expected sharp XRD peaks. The partially crystalline films display broadened peaks indicating disorder and/or small crystal grain sizes. The only peaks apparent in the spectra of the fully amorphous films were due to the sample holder and substrate on which several of the samples were grown. These features were absent

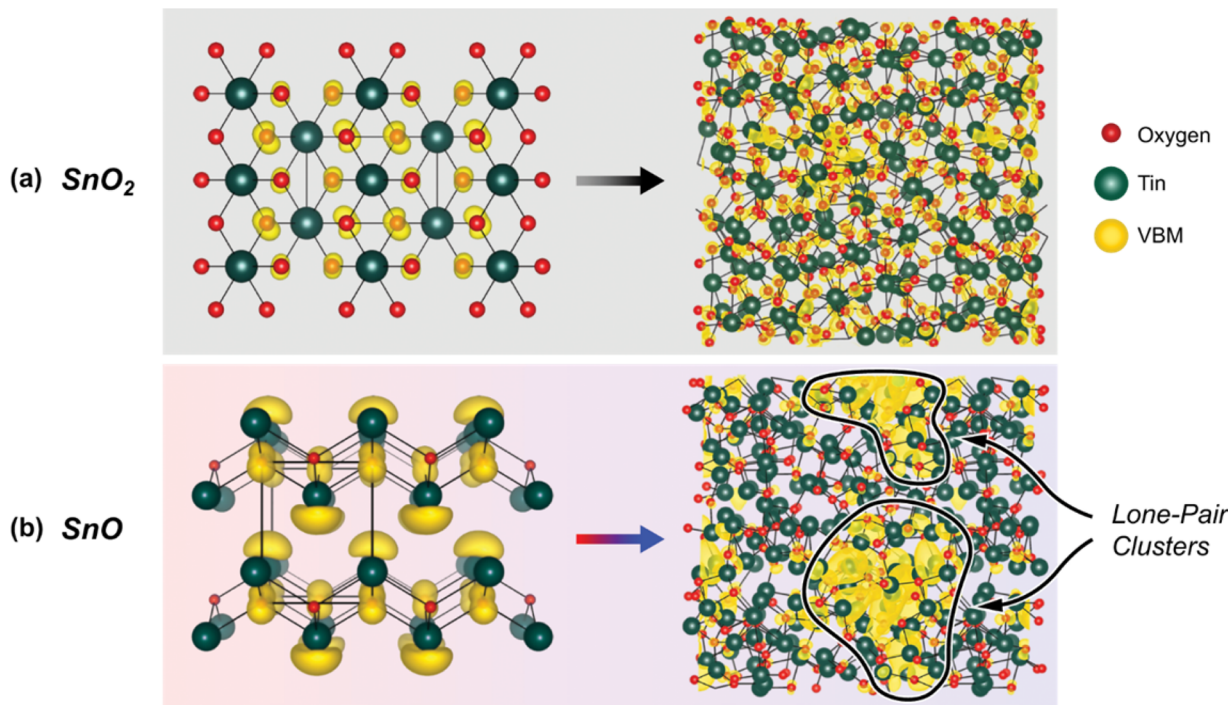


**Figure 6.** Spatial distribution of the VBM states (isosurfaces at  $5 \times 10^{-3} \text{ e}/\text{\AA}^3$ ) for crystalline and amorphous (a)  $\text{SnO}_2$  and (b)  $\text{SnO}$ .

when amorphous substrates were used and the samples were large enough to fully encompass the X-ray beam.

**UV–Visible Spectroscopy.** Optical transmittance and reflectance spectra were measured with a Filmetrics F20 series reflectometer with a T-1-UV transmittance upgrade. Fabry-Pérot oscillations observed below the films' optical absorptions edges necessitated the inclusion of reflectance spectra in the Tauc plot analysis to determine accurate band gap values (see *Supporting Information*).

**Hall Measurements.** Hall measurements were performed on the films using an Ecopia HMS-5000 Hall Effect Measurement System with indium contacts. Partially crystalline SnO films were found to be p-type from Hall measurements, while the fully amorphous films could not be accurately measured by the system.

**X-ray Spectroscopy.** Soft X-ray photoelectron spectroscopy (XPS) was performed using a laboratory-based monochromated Al K $\alpha$  X-ray source with a hemispherical analyzer located in the Analytical and Diagnostics Laboratory (ADL) at Binghamton University. Measurements were performed with a pass energy of 23.5 eV, corresponding to an instrumental resolution of 0.51 eV, determined from analyzing the Fermi edge and Au 4f<sub>7/2</sub> peak of Au foil references.

The surface sensitive nature of XPS meant that additional care was employed for studying the SnO films because of possible surface oxidation.<sup>21</sup> SnO samples were transferred into the XPS chamber adjacent to the PLD chamber immediately after growth to minimize surface contamination and oxidation, with the exception of the highest crystallinity SnO and amorphous SnO<sub>2</sub> films, which display non-negligible surface contamination as a result (see *Supporting Information*). Spectral contributions from surface contamination were distinguished from those of the bulk material through comparison between XPS and HAXPES, which possesses an ~4× deeper probing depth.<sup>40</sup>

Hard X-ray photoelectron spectroscopy (HAXPES) measurements were performed at the National Institute of Standards and Technology (NIST) bending magnet beamline X24 at the National Synchrotron Light Source (NSLS) at Brookhaven National Laboratory. Measurements were performed at a 4 keV photon energy, with a pass energy of 500 eV and a Gaussian instrumental broadening of 0.45 eV, comparable instrumental resolution to the laboratory-based XPS at the ADL. The higher photon energies utilized for HAXPES increased our effective probing depth to 12–15 nm versus only 3–4 nm for XPS.

Binding energy calibration of the data was performed using Au references, as internal references such as the carbon 1s peak proved unreliable.<sup>41</sup>

**Computation.** All DFT calculations were preformed using the Vienna Ab Initio Simulation Package (VASP)<sup>42</sup> within the projector augmented wave formalism.<sup>43,44</sup> To represent the electron density, a plane wave basis with a cutoff energy of 400 eV was used, and we employed the PBEsol exchange and correlation functional for molecular dynamics.<sup>45</sup> Molecular dynamics simulations were performed using the Gamma point only k-point sampling. The structures were obtained by melting the crystal phase at 3000 K, followed by cooling to 0 K at a rate of  $5 \times 10^{13} \text{ K s}^{-1}$ .<sup>46</sup> In the final structure, the volume and ionic degrees of freedom were relaxed. The crystalline structures were optimized with the same functional with a cutoff energy of 500 eV, using the k-point density sampling as prescribed by Moreno and Soler.<sup>47</sup> For the calculation of the electronic structure a degree of exact exchange was included using the HSE functional.<sup>48</sup> All structure analysis was performed using the R.I.N.G.S. code.<sup>49</sup> Once the effects of experimental broadening and orbital sensitivity were applied to the resultant calculated DOS<sup>32</sup> and the energy axes were manually aligned with those of the experimental data, excellent agreement was observed between measured and theoretical electronic structure.

## ■ ASSOCIATED CONTENT

### S Supporting Information

The Supporting Information is available free of charge on the ACS Publications website at DOI: [10.1021/acs.chemmater.6b01608](https://doi.org/10.1021/acs.chemmater.6b01608).

Additional XRD spectra, discussion of surface contamination, soft X-ray photoelectron and X-ray absorption spectra and additional analysis, additional optical analysis and details, DFT analysis details, and pair distribution function/bond angle distribution details ([PDF](#))

## ■ AUTHOR INFORMATION

### Corresponding Authors

\*E-mail: [ktb22@bath.ac.uk](mailto:ktb22@bath.ac.uk) (K.T. Butler).

\*E-mail: [lpiper@binghamton.edu](mailto:lpiper@binghamton.edu) (L.F.J. Piper).

**Present Addresses**

▽ Department of Chemistry, Massachusetts Institute of Technology, Cambridge, Massachusetts 02139, United States (C.H. Hendon).

◆ Department of Physics, University of South Florida, Tampa, Florida 33620, United States (D.A. Arena).

**Notes**

The authors declare no competing financial interest.

**ACKNOWLEDGMENTS**

The research at Binghamton was partially supported by the National Science Foundation under Grant No. DMR-1409912. K.M. acknowledges support from an NSF REU under Grant No. DMR-1263004. Use of the National Synchrotron Light Source, Brookhaven National Laboratory, was supported by the U.S. Department of Energy, Office of Science, Office of Basic Energy Sciences, under Contract No. DE-AC02-98CH10886. The Advanced Light Source is supported by the Director, Office of Science, Office of Basic Energy Sciences, of the U.S. Department of Energy under Contract No. DE-AC02-05CH11231. The research at Bath was supported by EPSRC grants: EP/K016288/1 and EP/J017361/1. The research at Trinity College Dublin was supported by SFI Grant 12/IA/1414. We also acknowledge PRACE for awarding us access to resource ARCHER based in the U.K. We thank Ken Durose for access to his laboratory facilities supported by EPSRC EP/K005901/1. The work of H.P. and D.G.S. was supported by the Center for Low Energy Systems Technology (LEAST), one of six centers of STARnet, a Semiconductor Research Corporation program sponsored by MARCO and DARPA. This work was performed in part at the Cornell NanoScale Facility, a member of the National Nanotechnology Coordinated Infrastructure (NNCI), which is supported by the National Science Foundation (Grant ECCS-1542081).

**REFERENCES**

- (1) Schirmer, O. F. Bound Small Polarons in Oxide Materials. *J. Phys.: Condens. Matter* **2006**, *18*, R667–R704.
- (2) Lany, S.; Zunger, A. Polaronic Hole Localization and Multiple Hole Binding of Acceptors in Oxide Wide-Gap Semiconductors. *Phys. Rev. B: Condens. Matter Mater. Phys.* **2009**, *80*, 085202.
- (3) Nomura, K.; Ohta, H.; Takagi, A.; Kamiya, T.; Hirano, M.; Hosono, H. Room-Temperature Fabrication of Transparent Flexible Thin-Film Transistors Using Amorphous Oxide Semiconductors. *Nature* **2004**, *432*, 488–492.
- (4) Robertson, J.; Clark, S. J. Limits to Doping in Oxides. *Phys. Rev. B: Condens. Matter Mater. Phys.* **2011**, *83*, 075205.
- (5) Walukiewicz, W. Intrinsic Limitations to the Doping of Wide-Gap Semiconductors. *Phys. B* **2001**, *303*, 123–134.
- (6) Scanlon, D. O.; Watson, G. W. On the Possibility of p-Type SnO<sub>2</sub>. *J. Mater. Chem.* **2012**, *22*, 25236–25245.
- (7) Kawazoe, H.; Yasukawa, M.; Hyodo, H.; Kurita, M.; Yanagi, H.; Hosono, H. P-Type Electrical Conduction in Transparent Thin Films of CuAlO<sub>2</sub>. *Nature* **1997**, *389*, 939–942.
- (8) Scanlon, D. O.; Watson, G. W. Conductivity Limits in CuAlO<sub>2</sub> from Screened-Hybrid Density Functional Theory. *J. Phys. Chem. Lett.* **2010**, *1*, 3195–3199.
- (9) Benko, F. A.; Koffyberg, F. P. Opto-Electronic Properties of CuAlO<sub>2</sub>. *J. Phys. Chem. Solids* **1984**, *45*, 57–59.
- (10) Narushima, S.; Mizoguchi, H.; Shimizu, K. I.; Ueda, K.; Ohta, H.; Hirano, M.; Kamiya, T.; Hosono, H. A p-Type Amorphous Oxide Semiconductor and Room Temperature Fabrication of Amorphous Oxide p-n Heterojunction Diodes. *Adv. Mater.* **2003**, *15*, 1409–1413.
- (11) Schlupp, P.; Schein, F.; von Wenckstern, H.; Grundmann, M. All Amorphous Oxide Bipolar Heterojunction Diodes from Abundant Metals. *Adv. Electron. Mater.* **2015**, *1*, 1400023.
- (12) Schein, F.-L.; Von Wenckstern, H.; Frenzel, H.; Grundmann, M. ZnO-Based n-Channel Junction Field-Effect Transistor With Room-Temperature-Fabricated Amorphous p-Type ZnCo<sub>2</sub>O<sub>4</sub> Gate. *IEEE Electron Device Lett.* **2012**, *33*, 676–678.
- (13) Schein, F.-L.; Winter, M.; Böntgen, T.; Von Wenckstern, H.; Grundmann, M. Highly Rectifying p-ZnCo<sub>2</sub>O<sub>4</sub>/n-ZnO Heterojunction Diodes. *Appl. Phys. Lett.* **2014**, *104*, 022104.
- (14) Allen, J. P.; Scanlon, D. O.; Parker, S. C.; Watson, G. W. Tin Monoxide: Structural Prediction from First Principles Calculations with van Der Waals Corrections. *J. Phys. Chem. C* **2011**, *115*, 19916–19924.
- (15) Allen, J. P.; Scanlon, D. O.; Piper, L. F. J.; Watson, G. W. Understanding the Defect Chemistry of Tin Monoxide. *J. Mater. Chem. C* **2013**, *1*, 8194–8208.
- (16) Walsh, A.; Watson, G. Electronic Structures of Rocksalt, Litharge, and Herzenbergite SnO by Density Functional Theory. *Phys. Rev. B: Condens. Matter Mater. Phys.* **2004**, *70*, 235114.
- (17) Walsh, A.; Watson, G. W. Influence of the Anion on Lone Pair Formation in Sn(II) Monochalcogenides: A DFT Study. *J. Phys. Chem. B* **2005**, *109*, 18868–18875.
- (18) Walsh, A.; Payne, D. J.; Egddell, R. G.; Watson, G. W. Stereochemistry of Post-Transition Metal Oxides: Revision of the Classical Lone Pair Model. *Chem. Soc. Rev.* **2011**, *40*, 4455–4463.
- (19) Watson, G. W. Origin of the Electron Distribution in SnO. *J. Chem. Phys.* **2001**, *114*, 758–763.
- (20) Saji, K. J.; Tian, K.; Snure, M.; Tiwari, A. 2D Tin Monoxide — An Unexplored p-Type van Der Waals Semiconductor: Material Characteristics and Field Effect Transistors. *Adv. Electron. Mater.* **2016**, *2*, 1500453.
- (21) Quackenbush, N. F.; Allen, J. P.; Scanlon, D. O.; Sallis, S.; Hewlett, J. a.; Nandur, a. S.; Chen, B.; Smith, K. E.; Weiland, C.; Fischer, D. a.; Woicik, J. C.; White, B. E.; Watson, G. W.; Piper, L. F. J. Origin of the Bipolar Doping Behavior of SnO from X-Ray Spectroscopy and Density Functional Theory. *Chem. Mater.* **2013**, *25*, 3114–3123.
- (22) Ogo, Y.; Hiramatsu, H.; Nomura, K.; Yanagi, H.; Kamiya, T.; Kimura, M.; Hirano, M.; Hosono, H. Tin Monoxide as an s-Orbital-Based p-Type Oxide Semiconductor: Electronic Structures and TFT Application. *Phys. Status Solidi A* **2009**, *206*, 2187–2191.
- (23) Guo, W.; Fu, L.; Zhang, Y.; Zhang, K.; Liang, L. Y.; Liu, Z. M.; Cao, H. T.; Pan, X. Q. Microstructure, Optical, and Electrical Properties of p-Type SnO Thin Films. *Appl. Phys. Lett.* **2010**, *96*, 042113.
- (24) Sallis, S.; Butler, K. T.; Quackenbush, N. F.; Williams, D. S.; Junda, M.; Fischer, D. A.; Woicik, J. C.; Podraza, N. J.; White, B. E.; Walsh, A.; Piper, L. F. J. Origin of Deep Subgap States in Amorphous Indium Gallium Zinc Oxide: Chemically Disordered Coordination of Oxygen. *Appl. Phys. Lett.* **2014**, *104*, 232108.
- (25) Sallis, S.; Quackenbush, N. F.; Williams, D. S.; Senger, M.; Woicik, J. C.; White, B. E.; Piper, L. F. J. Deep Subgap Feature in Amorphous Indium Gallium Zinc Oxide: Evidence against Reduced Indium. *Phys. Status Solidi A* **2015**, *212*, 1471–1475.
- (26) Körner, W.; Urban, D. F.; Elsässer, C. Generic Origin of Subgap States in Transparent Amorphous Semiconductor Oxides Illustrated for the Cases of In-Zn-O and In-Sn-O. *Phys. Status Solidi A* **2015**, *212*, 1476–1481.
- (27) Fortunato, E.; Barquinha, P.; Martins, R. Oxide Semiconductor Thin-Film Transistors: A Review of Recent Advances. *Adv. Mater.* **2012**, *24*, 2945–2986.
- (28) Hayashi, H.; Katayama, S.; Huang, R.; Kurushima, K.; Tanaka, I. Selective Fabrication of n- and p-Type SnO Films without Doping. *Phys. Status Solidi RRL* **2015**, *9*, 192–196.
- (29) Mott, N. F. Oxford science publications; *Conduction in Non-Crystalline Materials*; Oxford science publications; 1987.

- (30) Wang, J.; Umezawa, N.; Hosono, H. Mixed Valence Tin Oxides as Novel van Der Waals Materials: Theoretical Predictions and Potential Applications. *Adv. Energy Mater.* **2016**, *6*, 1501190.
- (31) Hanyš, P.; Janeček, P.; Matolin, V.; Korotcenkov, G.; Nehasil, V. XPS and TPD Study of Rh/SnO<sub>2</sub> System – Reversible Process of Substrate Oxidation and Reduction. *Surf. Sci.* **2006**, *600*, 4233–4238.
- (32) Scofield, J. H. *Theoretical Photoionization Cross Sections from 1 to 1500 keV*; Lawrence Livermore Laboratory, U.S. Atomic Energy Commission: 1973.
- (33) Körner, W.; Elsässer, C. Density-Functional Theory Study of Stability and Subgap States of Crystalline and Amorphous Zn-Sn-O. *Thin Solid Films* **2014**, *555*, 81–86.
- (34) Zhu, Q.; Ma, Q.; Buchholz, D. B.; Chang, R. P. H.; Bedzyk, M. J.; Mason, T. O. Structural Anisotropy in Amorphous SnO<sub>2</sub> Film Probed by X-Ray Absorption Spectroscopy. *Appl. Phys. Lett.* **2013**, *103*, 031913.
- (35) Zhou, W.; Umezawa, N. Band Gap Engineering of Bulk and Nanosheet SnO: Insight into the Interlayer Sn-Sn Lone Pair Interactions. *Phys. Chem. Chem. Phys.* **2015**, *17*, 17816–17820.
- (36) Buchholz, D. B.; Ma, Q.; Alducin, D.; Ponce, A.; Jose-yacaman, M.; Khanal, R.; Medvedeva, J. E.; Chang, R. P. H. The Structure and Properties of Amorphous Indium Oxide. *Chem. Mater.* **2014**, *26*, 5401–5411.
- (37) Podzorov, V. Conjugated Polymers: Long and Winding Polymeric Roads. *Nat. Mater.* **2013**, *12*, 947–948.
- (38) Elschner, A.; Kirchmeyer, S.; Lovenich, W.; Merker, U.; Reuter, K. *PEDOT: Principles and Applications of an Intrinsically Conductive Polymer*; CRC Press: 2010.
- (39) Germs, W. C.; Adriaans, W. H.; Tripathi, A. K.; Roelofs, W. S. C.; Cobb, B.; Janssen, R. A. J.; Gelinck, G. H.; Kemerink, M. Charge Transport in Amorphous InGaZnO Thin-Film Transistors. *Phys. Rev. B: Condens. Matter Mater. Phys.* **2012**, *86*, 155319.
- (40) Wahila, M. J.; Lebens-Higgins, Z. W.; Quackenbush, N. F.; Nishitani, J.; Walukiewicz, W.; Glans, P.; Guo, J.; Woicik, J. C.; Yu, K. M.; Piper, L. F. J. Evidence of Extreme Type-III Band Offset at Buried n-Type CdO/p-Type SnTe Interfaces. *Phys. Rev. B: Condens. Matter Mater. Phys.* **2015**, *91*, 205307.
- (41) Barr, T. L.; Seal, S. Nature of the Use of Adventitious Carbon as a Binding Energy Standard. *J. Vac. Sci. Technol., A* **1995**, *13*, 1239–1246.
- (42) Kresse, G.; Furthmüller, J. Efficient Iterative Schemes for Ab Initio Total-Energy Calculations Using a Plane-Wave Basis Set. *Phys. Rev. B: Condens. Matter Mater. Phys.* **1996**, *54*, 11169–11186.
- (43) Blöchl, P. E. Projector Augmented-Wave Method. *Phys. Rev. B: Condens. Matter Mater. Phys.* **1994**, *50*, 17953–17979.
- (44) Kresse, G.; Joubert, D. From Ultrasoft Pseudopotentials to the Projector Augmented-Wave Method. *Phys. Rev. B: Condens. Matter Mater. Phys.* **1999**, *59*, 1758–1775.
- (45) Perdew, J. P.; Ruzsinszky, A.; Csonka, G. I.; Vydrov, O. A.; Scuseria, G. E.; Constantin, L. A.; Zhou, X.; Burke, K. Restoring the Density-Gradient Expansion for Exchange in Solids and Surfaces. *Phys. Rev. Lett.* **2008**, *100*, 136406.
- (46) Butler, K. T.; Lamers, M. P. W. E.; Weeber, A. W.; Harding, J. H. Molecular Dynamics Studies of the Bonding Properties of Amorphous Silicon Nitride Coatings on Crystalline Silicon. *J. Appl. Phys.* **2011**, *110*, 124905.
- (47) Moreno, J.; Soler, J. M. Optimal Meshes for Integrals in Real- and Reciprocal-Space Unit Cells. *Phys. Rev. B: Condens. Matter Mater. Phys.* **1992**, *45*, 13891–13898.
- (48) Krukau, A. V.; Vydrov, O. A.; Izmaylov, A. F.; Scuseria, G. E. Influence of the Exchange Screening Parameter on the Performance of Screened Hybrid Functionals. *J. Chem. Phys.* **2006**, *125*, 224106.
- (49) Le Roux, S.; Jund, P. Ring Statistics Analysis of Topological Networks: New Approach and Application to Amorphous GeS<sub>2</sub> and SiO<sub>2</sub> Systems. *Comput. Mater. Sci.* **2010**, *49*, 70–83.